Proceedings of ICFDP2006
International Congress of Fluid Dynamics propulsion
December 14-17, 2006 Sharm El-Shiekh, Sinai, Egypt

ICFDP8-EG-127

Numerical Investigation of Buoyancy-Driven Cavity with Different Mediums and Temperature Differences

Ismail Mohamed sakr
Mechanical Power Eng. Dept.
Faculty of Engineering-Menoufia Uni.
Shebin El-kom-Egypt
Email: ismailsakr@yahoo.com

Ashraf Balabel
Mechanical Power Eng. Dept.
Faculty of Engineering-Menoufia Uni.
Shebin El-kom-Egypt
Email: ashrafbalable@yahoo.com

Abdelkarim Hegab
Mechanical Power Eng. Dept.
Faculty of Engineering-Menoufia Uni.
Shebin El-kom-Egypt
Email: hegab2002us@yahoo.com

Sobeih Selim
Mechanical Power Eng. Dept.
Faculty of Engineering-Menoufia Uni.
Shebin El-kom-Egypt
Email: sobhselim@yahoo.com

ABSTRACT

The comprehensive analysis of the fluid flow and heat transfer patterns inside the buoyancy-driven square cavities is a necessary precursor to the evolution of better designs for more complex industrial applications. In the present paper, a focused study on the problem of the buoyancy-driven cavity with different working mediums and a wide range of thermal properties is presented. The adopted numerical method is based on the solution of the complete Navier-Stokes and energy equations using the finite volume technique employing SIMPLE algorithm on a staggered grid. The buoyancy forces are represented using the Boussinesq approximation. The present scheme is used to generate benchmark-quality data for the entire laminar and transient natural-convection-Rayleigh number range of $10^3 \leq Ra \leq 10^9$ for different working mediums having a wide rang of Prandtl number (0.71, 10.0, 210.5 and 11648.57). Consequently, an elaborate analysis of the heat transfer process in such cavities is obtained. A comparison between the obtained numerical results and the available ones from a number of other computational schemes is also presented.

Keywords: Numerical simulation, buoyancy-driven cavity, natural convection, laminar/transient flow

NOMENCLATURE

C_p Specific heat (J/kg.K)

T_H Hot wall temperature (^oC)

g Acceleration due to gravity (m/s^2)

T_C Cold wall temperature (^oC)

Gr Grashof number

ΔT Temperature difference

P_r Prandtl number

k Thermal conductively (W/m.K)

Ra Rayleigh number

α Thermal diffusivity of the fluid (m^2/s)

u^* Dimensionless horiz. Velocity (=uL/α)

β Coefficient of thermal expansion (k^{-1})

v^* Dimensionless vert. velocity(=vL/α)

θ Dimensionless temperature [= (T- T_C)/(T_H- T_C)]

X^* Dimensionless horiz. Coordinate (=x/L)

Y^* Dimensionless vert. coordinate (=y/L)

ρ Density (kg/m^3)

υ Kinematics viscosity (m^2/s)

INTRODUCTION

Natural convection heat transfer inside cavities has been subjected to several studies in the last years. The attention is due to the wide range of real-world applications such as building insulation, solar cavity receivers, ventilation and the cooling of electrical components, nuclear reactors, heat–recovery system, crystal growth in liquids, multi-pane

windows and solidification in castings, etc. Consequently, a comprehensive analysis of the fluid flow and heat transfer patterns in fundamentally simple geometries, such as the buoyancy-driven square cavity, is a necessary precursor to the evolution of better designs for more complex industrial applications. The fluid flow and heat transfer behavior of such systems can be predicted by the conservation equations of mass, momentum and energy with appropriate boundary conditions. The fast-emerging branch of computational fluid dynamics (CFD) facilitates the numerical simulation of fluid flow and heat transfer features.

In the early 1980s, this problem was solved by a number of different groups and their results were extensively summarized in the standard reference by de Vahl Davis and Jones [1]. De Vahl Davis [2] provided numerically benchmark data for the thermal driven square cavity flow with Boussinesq approximation at Prandtl number of 0.71. The cavity was subjected to null velocity components at the boundary and thermally heated vertical walls and isolated horizontal. He employed an alternating direction implicit algorithm with second-order central differences and Richardson extrapolation within the vorticity-stream formulation. Although the solution obtained was among the best of those days, the data presented were limited to a value of Rayleigh number up to 10^6.

Afterwards, a variety of computational algorithms has been tested on this problem and the vast amount of literature is a testimony to this [1-10]. For example, Hortmann et al. [4] have employed a finite-volume-based multigrid technique for the simulation of a buoyancy-driven cavity. Ramaswamy et al. [8] have investigated the performance of two explicit and one semi-implicit projection-based scheme. They have concluded that the semi-implicit scheme always outperforms the two explicit schemes considered by them. In their numerical investigations, a variety of benchmark problems were solved, including the buoyancy driven cavity. Shu and Xue [9] employed a global method of generalized differential quadrature (GDQ) for solving the stream function-vorticity form of the Navier-Stokes equations. Massarotti et al. [6] used a semi-implicit form of the characteristic-based split scheme (CBS) with equal-order interpolation functions for all the variables. Manzari et al. [7] developed an artificial diffusion-based algorithm for 3-D compressible turbulent flow problems. This was later extended to 2-D laminar heat transfer problems. The basic idea of Manzari et al. [7] involves modification of continuity equation by employing the concept of artificial compressibility.

Recently, Mayne et al. [10] employed an *h*-adaptive finite-element method to ensure a very accurate solution for the thermal cavity problem. Recently, Wan et al. [12] have introduced a high-accuracy discrete singular convolution (DSC) for the numerical simulation of coupled convective heat transfer problems. They used a quasi-wavelet-based (DSC) approach, which uses the regularized Shannon's kernel, to solve the problem of the buoyancy- driven cavity. The reliability and robustness of the (DSC) approach are extensively tested and validated by means of grid sensitivity and convergence studies. The study emphasizes quantitative, rather than qualitative comparisons.

Despite so much effort on this problem, there still exist some variations and discrepancies in the available literature. Inherently, numerical results are approximations. Their accuracy and reliability depends vitally on the underlying computational method and the numerical scheme. Hence, further advances in computational methodology are crucial to the thermal cavity problem as well as other heat transfer problems.

The present study presents a description of the mathematical formulation for the natural convection square cavity starting from the basic governing equations and the formulation of the boundary conditions. A brief description of the essential features of numerical techniques developed used for solving the appropriate system of equations is presented. In addition, the effect of varying the Prandtl number associated for various working fluids such as air, water, glycerin and ethylene glycol for the buoyancy- driven cavity is presented.

The buoyancy force generated due to density differences in convection problem is being to compete with the inertia and viscous force. Therefore, a number of non-dimensional numbers are characterizing the flow, namely Rayleigh, Prandtl, and Grashof number. They are defined as follows:

$$Ra = \frac{g\beta\Delta T L^3}{\nu\alpha}, \quad Pr = \frac{\nu}{\alpha}, \quad Gr = \frac{Ra}{Pr} \qquad (1)$$

The ratio of buoyancy to viscous forces is given by the Grashof number (**Gr**), which controls natural convection.

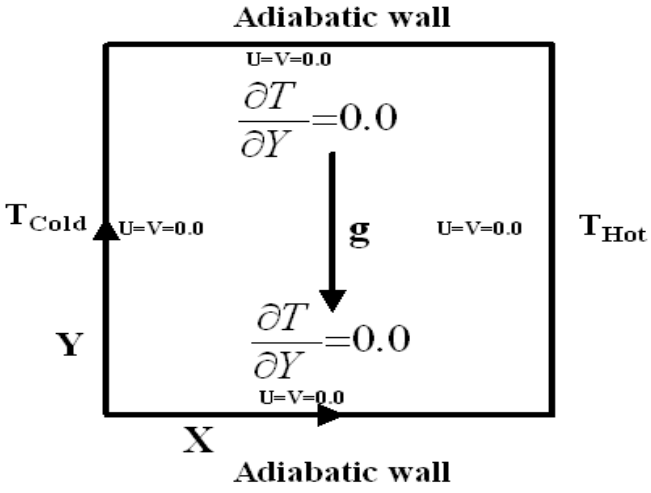

Figure 1.Flow domain and boundary conditions.

On the other hand, the ratio of momentum to thermal diffusivity, known as Prandtl number (**Pr**), which governs the temperature field and its relationship with the fluid flow characteristics. Rayleigh number (**Ra**), which is the parameter of interest, is the product of these two dimensionless groups**.**

PROBLEM DESCRIPTION

A differentially heated, closed square cavity is illustrated in figure 1. The left and right vertical walls are maintained at T_C

and T_H, respectively. The horizontal walls are adiabatic (insulated, and there is no transfer of heat through these walls). The confined medium is assumed to be viscous, incompressible, Newtonian, and Boussinesq approximated. The Boussinesq approximation means that the density differences are confined to the buoyancy term, without violating the assumption of incompressibility. It should be pointed out that there is an additional coupling term in the momentum equations, which indeed dictates the fluid motion within the cavity. Different working mediums are used in the present study, namely air, water, glycerin, and ethylene glycol. Their properties are shown in Table (1).

Table (1) Mediums properties

Medium	Air	Water	Ethylene Glycol	Glycerin
ρ [kg/m^3]	1.194	998.4	117.48	1263.27
μ [Pa.s]	18.2E-6	1007E-6	2.2E-2	139.9E-2
$\boldsymbol{\beta}$ [1/***k***]	0.00341	206.1E-6	0.65E-3	0.48E-3
C_p [J/kg.K]	1007.0	4182.2	2.38E3	2392.7
k [W/m.K]	25.74E-3	602E-3	249.2E-3	286E-3
P_r	0.71	7.0	210.5	11648.5

MATHEMATICAL FORMULATION:

Governing Equations:

The field equations and the subsequent fluid motion inside the cavity can be described by the continuity, momentum and energy equations. In vector form, are:

$$\nabla \cdot \mathbf{u} = 0$$
$$\rho \mathbf{u} \cdot \nabla \mathbf{u} + \nabla p - \mu \nabla^2 \mathbf{u} - \rho g \beta (T - T_{ref}) = 0 \qquad (2)$$
$$\rho C_p \mathbf{u} \cdot \nabla T - k \nabla^2 T = 0$$

These equations assume steady state flow and an incompressible fluid with negligible viscous dissipation. The domain of the cavity is two-dimensional rectangular geometry with equally grid spacing. A uniform staggered grid with different numbers of control volumes was firstly used in order to test the solution-grid independence. It was observed that, fine grid must be used for flow with high Rayleigh number in order to accurately capture the thermal flow characteristics. Therefore, the grid size of 256x256 is used for all cases to ensure the results accuracy over the considered Rayleigh number range.

Boundary Conditions

The boundary conditions of the problem under consideration are illustrated in figure 1, where no-slip boundary condition ($u = v = 0$) is applied on all four walls of the square cavity. Dirichlet boundary conditions of T_C and T_H are enforced on the left and right vertical walls, respectively. A Neumann boundary condition ($\partial T / \partial y = 0.0$), is applied, through the horizontal walls, since there is no transfer of heat.

Numerical Procedure

The numerical procedure adopted here is essentially based on the finite volume method proposed by Patankar [15]. The SIMPLE algorithm was applied to resolve the pressure-velocity coupling in the momentum equation. The temperature and the velocity field are coupled through the buoyancy force approximation. For more details about the numerical procedure and the consequence of the calculations, one can see [15].

VALIDATION OF NUMERICAL METHOD

The buoyancy driven flow in a differentially heated closed square cavity has been proposed as a suitable vehicle for testing and validating computer codes for thermal problems. This problem is firstly performed to illustrate the capability of the numerical solution to predict the thermal characteristics at different values of Rayleigh number in the case of Prandtl number of 0.71. The numerical results obtained are compared with the available results of Wan et al. [12], which provide a set of new benchmark quality data for this problem.

Figures (2-a), (2-b) show the variation of both horizontal and vertical velocities at the mid-width ($x^*=0.5$), and the mid-height ($y^*=0.5$), respectively. The low range of Rayleigh number ranged from 10^3 to 10^6 is shown in the upper curves, while the high range of **Ra** from 10^7 to 10^9 is shown in the lower curves.

The comparison shows that an excellent agreement is found in case of low **Ra** for both horizontal and vertical velocity components. However, for high **Ra**, a little deviation is found especially for the vertical velocity component near the boundary. The reason behind that may be related to the direct relation between the vertical velocity distribution and the size of the boundary layer formed on the hot and cold walls. The boundary layer is more closely confined to the vertical walls by increasing the Rayleigh number. Consequently, at this point, we can conclude that, a fine grid resolution should be used to resolve the boundary layer in the wall regions. Nevertheless, it should be pointed out that both numerical results yield similar peak value positions.

The calculation of **Ra**=10^9 is not included by Wan et al.[12], but here it is performed in order to show that the laminar natural convection at this local Rayleigh number may be approached to turbulent transition in the vertical boundary layer. This is evident through the oscillation observed in the horizontal velocity component. This phenomenon has also been observed and discussed by Incropera and Dewitt [11].

RESULTS AND DISCUSSION

A wide variety of fluid flow and heat transfer features evolve as a function of the Rayleigh number and their precise simulation is indeed a real challenge to any numerical scheme. In this section, the computational results for a wide range of Rayleigh number $10^3 \leq$ **Ra** $\leq 10^9$ and for different working mediums are presented and discussed. The different working mediums used are treated as incompressible and Newtonian fluids in the range of Rayleigh number considered. This assumption enables us to investigate the dependence of the flow as function of prandle number according to the material type. Once again, the properties of the different mediums used in our numerical experiments, namely; air, water, glycerin and ethylene glycol are illustrated in Table 1. In all cases, the fluid inside the cavity is initially maintained at the same temperature, say the mean temperature. The fluid picks up heat from the hot wall and gives it to the cold wall. There is no transfer of heat through the horizontal walls (either inside or outside).

Velocity Distribution

The vertical velocity distribution at the mid-height ($y^*=0.5$) as a function of the abscissa for the working mediums considered here is presented in figures (3-a), (3-b) over a wide range of Rayleigh number $10^3 \leq$ **Ra** $\leq 10^9$.

For low **Ra**-regime, figure (3-a), the vertical velocity distribution for all mediums is nearly similar at the same Rayleigh number. Moreover, the distribution indicates that, the boundary layer is more closely confined to the vertical walls with the increase of the Rayleigh number. This behavior leads to the movement of the position of maximum velocity close to the solid walls. In addition, there is a reasonable increase in the maximum vertical velocity by increasing the Rayleigh number. An important feature of the illustrated velocity profiles can be observed, namely the distribution is symmetric with respect to mid-height ($y^*=0.5$).

For high **Ra**-regime, figure (3-b), the same behavior of increasing the maximum velocity by increasing the Rayleigh number is also obtained. However, the velocity profile, in contrary to the low **Ra**-regime, shows asymmetric distribution where the boundary layer is formed only on the cold wall. In other words, the large temperature difference between the cold and hot sides revealed that the flow may behave as a boundary layer flow, i.e. the gradient of the vertical velocity component increases near the cold wall and it is vanished near the hot wall. These figures reveal also that, the **Ra**-number has not only a great effect on the thermal boundary layer thickness, but also on the formation of these thermal boundary layers.

The variation of horizontal velocity at the mid-width against the ordinate for the different working mediums considered is presented in figures (4-a), (4-b) for low and high Rayleigh number regimes, respectively. These figures show the intensity and the direction of fluid motion to be between the left and right zones of the square cavity. Only sample profiles are illustrated.

For low **Ra**-regime, figure (4-a), the horizontal velocity profiles for all working mediums shows a symmetric behavior around the mid-width ($x^*=0.5$). It should be particularly noted that the maximum horizontal velocity does not occur along or close to the mid-height, but rather is noticed at a point close to the top left- and the bottom right corner of the cavity. This phenomenon can be clearly observed by increasing the **Ra** number as the maximum horizontal velocity also increases.

In figure (4-b), the horizontal velocity profiles at high **Ra** – regime are illustrated. The profiles indicate that the symmetric behavior is found to be similar to that of low Ra-regime. Moreover, the high increases of **Ra**, the high increase of the maximum values of velocity. It is noted also that, these symmetric characteristics for air and water intend to break down if the **Ra** approaches to 10^9. The reason behind that is related to the increase of the velocity fluctuations which may, in turn, approaches to turbulent characteristics. In contrast, in case of glycerin, the profile remains symmetric and does not respond well to $Ra=10^9$ as in case of air and water. The contribution of the large value of the dynamics viscosity of glycerin may lead to damping the resulting irregular flow oscillations. Therefore, the flow regime can be considered to be laminar for the high viscosity mediums even for large values of Rayleigh number.

Thermal Distribution

Knowledge of heat transfer coefficient along the hot and cold walls is invaluable to thermal engineers and designers. Nusselt number (**Nu**) represents the desired nondimensional parameter of interest, which is the ratio of heat convected from the wall to the fluid, to that conducted up to the wall. The local Nusselt number can be defined as:

$$Nu_{local} = \pm \frac{\partial \Theta}{\partial X}\Big|_{wall} \qquad (3)$$

The positive sign in the above relation essentially implies transfer of heat is from the hot wall to the fluid, while a negative sign means from the fluid to the cold wall. Local Nusselt number distribution, generated by the present code, is compared; in figure 5, with the results of Refs. [6, 12]. It can be seen that, the pattern of distribution in low-**Ra** range differs significantly from that at high-**Ra** range. At low-**Ra** range $10^3 \leq$ **Ra** $\leq 10^4$, the results show reasonable agreements with both previous data. In contrary to that, i.e. at $Ra=10^5$, it is noted that , the results obtained are found to be very close to the results of Wan et al. [12], while a significant deviation from that of Massarotti et al.[6] is observed. Moreover, the reasonable comparison between the results obtained from the current code and that by Wan et al. [12] is continued to the **Ra** number up to 10^6. For **Ra** value lager than 10^6, the present results differ significantly from- and over predict both previous data. Nevertheless, this aspect has been confirmed by other numerical schemes (Wan et al. [12]). Despite the apparent simplicity in the geometry, clarity in the boundary conditions, the phenomenal progress made in computational methods, and the fast-growing number-crunching capability, there is a wide variation among the investigations, even in the prediction of a simple design parameter (**Nu**). This lack of agreement poses a hindrance to the reliable simulation of more complex, industrial scale fluid flow and heat transfer

problems. Further, it is also emphasizes the need to resolve this aspect by other independent numerical investigations.

Figures (6-a) and (6-b) elucidate the distribution of the local Nusselt number along the cold and hot walls for different **Ra** number. It is natural to expect an antisymmetric local **Nu** distribution between the cold and hot walls, as there exists a steady-state asymmetric distribution in the fluid flow and heat transfer patterns. This aspect can be noticed from the figures. There is a greater transfer of heat from the lower top of the hot wall to the fluid. Also, the lower bottom portion of the cold wall picks up more heat from the fluid. This rate of transfer of heat from the wall to the fluid, and vice versa, increases with the increase of Rayleigh number. Local Nu is maximum at a point close to the bottom of the hot wall and minimum at the top. On the cold wall, it is minimum at the bottom and maximum at a point close to the top wall. The same trend of **Nu** can also be observed at high **Ra**, in addition to some disturbances due to the **Ra** number increasing.

Figure (7–a) presents the dimensionless temperature variation at the mid-height, against the abscissa (only near the hot wall boundary is plotted). The results firstly are compared with those of Wan et al. [12] and good agreement is obtained. For the other working mediums, figures (7-b), (7- c), and (7-d), a slightly difference in the temperature amplitude is observed while the same trend is retained. Clearly, it can be seen that, for low **Ra** the temperature distribution is almost linear, however, this linearity is changed considerably by increasing the **Ra** number for all mediums.

Conclusions

The present study has introduced a new benchmark quality data of the coupled convection heat transfer problem in a square cavity with different working mediums and thermal operating conditions. The numerical investigation is based on the solution of the complete Navier-Stokes and energy equations using a finite volume technique employing SIMPLE algorithm on staggered grids, while the buoyancy force is represented using the Boussinesq approximation. A comparative study of the results obtained from other computation schemes is also presented. Generally, the comparison revealed that the present code could predict a very accurate problem solution at a reasonable computation cost. The effect of the Rayleigh number is clearly visible on the obtained results, where it can affect the characteristics of the thermal boundary layer formed on both cold and hot walls. Moreover, by changing the working mediums, or in other word changing the Prandtl number, the transient to turbulent flow is hindered by increasing the Prandtl number, in turn, indicating the important role of the viscous effects in such cases.

REFERENCES

[1] D. de Vahl Davis and I. P. Jones, 1983, "Natural Convection of Air in a Square Cavity: A Comparison Exercise" *Int. J. Numer. Meth. Fluids*, vol. 3, PP. 227± 248.

[2] D. de Vahl Davis, 1983, " Natural Convection of Air in a Square Cavity: A Bench Mark Solution," *Int. J. Numer. Meth. Fluids*, vol. 3, PP. 249± 264.

[3] I. P. Jones, 1979, "A Comparison Problem for Numerical Methods in Fluid Dynamics: The Double Glazing Problem, in R. W.Lewis and K. Morgan (eds.)," Numerical *Methods in Fluids* in Thermal Problems, PP. 338± 348, Pineridge Press, Swansea, UK.

[4] Hortmann, M., Peric, M., and Scheuerer, G., 1990, "Finite Volume Multi Grid Prediction of Laminar Natural Convection: Benchmark Solutions", Int. J. Numer. Meth. Fluids, Vol. 11, PP. 189-207.

[5] Le Quere, P.and De Roquefort, A., 1985, "Computation of Natural Convection in Two-Dimensional Cavities with Chebyshev Polynomials", Journal of Computational Physics, Vol. 57, PP. 210-28.

[6] N. Massarotti, P. Nithiarasu, and O. C. Zienkiewicz, 1998,"Characteristic-Based-plit (CBS) Algorithm for Incompressible Flow Problems with Heat Transfer", Int. J. Numer. Meth. Heat Fluid Flow, vol. 8, PP. 969± 990,.

[7] Manzari, M.T., Hassan, Morgan, O.K., and Weatherhill, N.P., 1998,"Turbulent Flow Computations on 3D Unstructured Grids", *Finite Elements Anal. Design*, Vol. 30, PP. 353-363.

[8] Ramaswamy, B., Jue, T. C., and Akin, J. E., 1992,"Semi-implicit and Explicit Finite lement Schemes for Coupled Fluid/Thermal Problems", Int. J. Numer. Meth. Eng., Vol. 34, PP. 675-696.

[9] Shu, C. and Xue, H., 1998,"Comparison of Two Approaches for Implementing Stream Function Boundary Conditions in DQ Simulation of Natural Convection in a Square Cavity", Int. J. *Heat Fluid Flow*, Vol. 19, PP. 59-68.

[10] Mayne, D.A., Usmani, A.S., and Crapper, M., , 2000, "*h*-Adaptive Finite Element Solution of High Rayleigh Number Thermally Driven Cavity Problem", Int. J. Numer. Meth. *Heat Fluid Flow*, Vol. 10, PP. 598-615.

[11] Incropera, F. P. and DeWitt, D. P., 1996,"*Fundamentals of Heat and Mass Transfer* 4thed" Wiley, New York..

[12] Wan, D.C., Patnaik, B.S.V., and Wei, G.W., 2001, "A New Benchmark Quality Solution for the Buoyancy-Driven Cavity by Discrete Singular Convolution", Numerical Heat Transfer, Part B, 40, PP.199-228.

[13] Miomir Raos, 2001,"Numerical investigation of laminar Natural Convection in Inclined Square Enclosures", Physics, Chemistry and Technology, vol. 2, N 3, PP.149-157.

[14] Safwat Mohamed, M., 2004,"Numerical simulation of Natural Convection of Air in a Square cavity: A benchmark test", IMECE, PP.560-573.

[15] Patankar, S.V., 1980, "*Numerical Heat Transfer and Fluid Flow*", McGraw-Hill, New York.

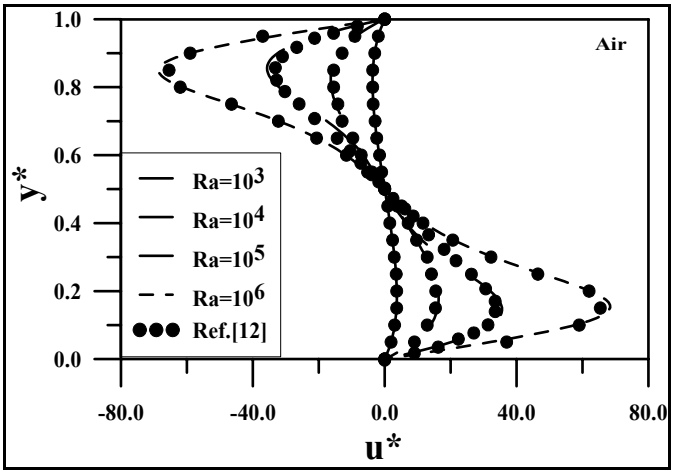

(a)

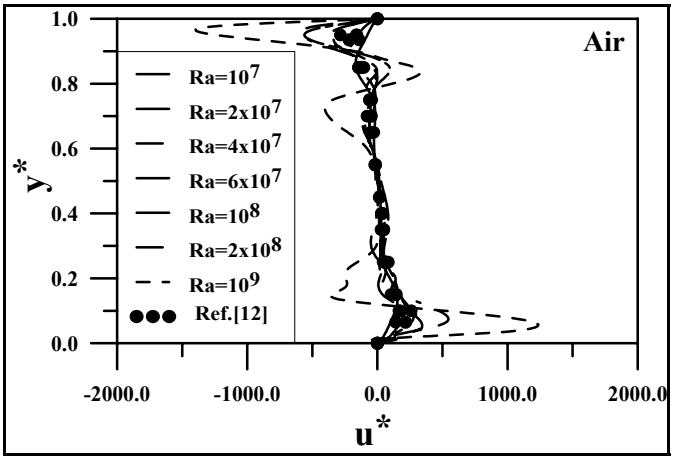

(a)

Figure 2: a)-Comparison of horizontal velocity at different Rayleigh numbers.

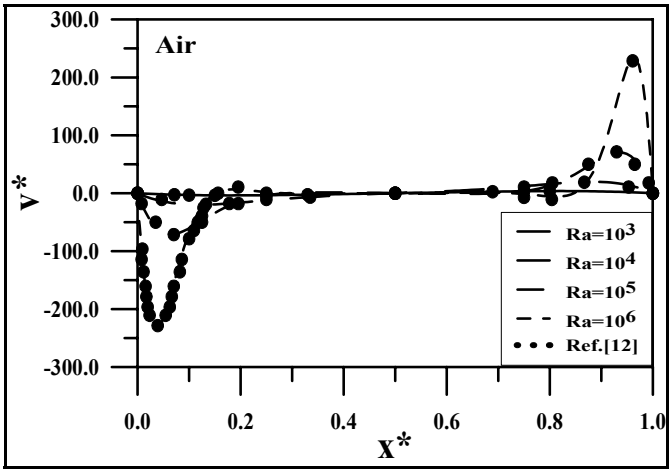

(b)

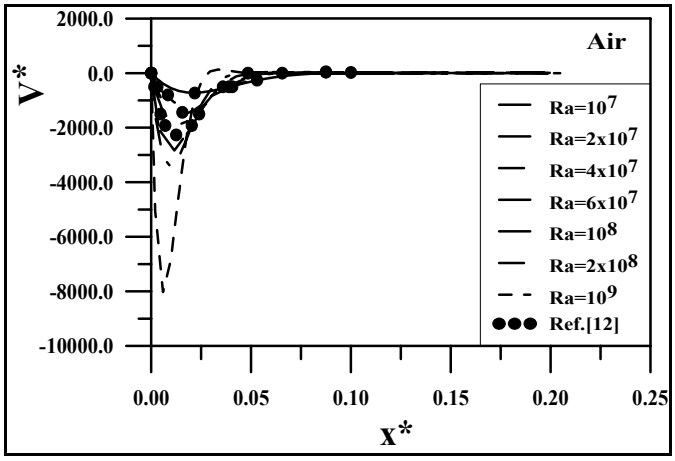

(b)

Figure 2: b)-Comparison of vertical velocity at different Rayleigh numbers.

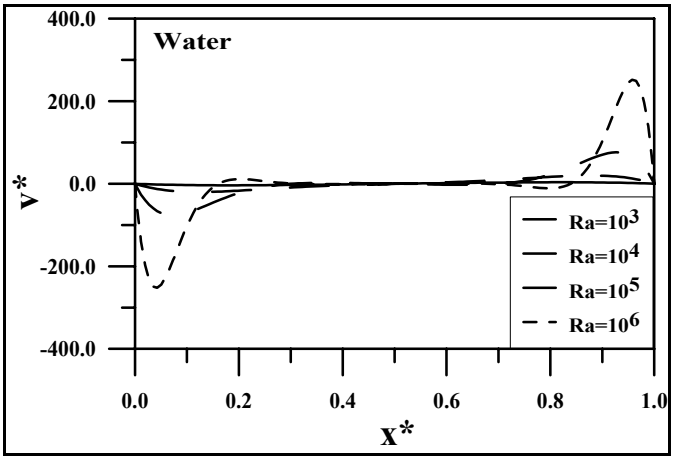

(a)

Figure 3: a)-Vertical Velocity distribution for low Rayleigh number regime.

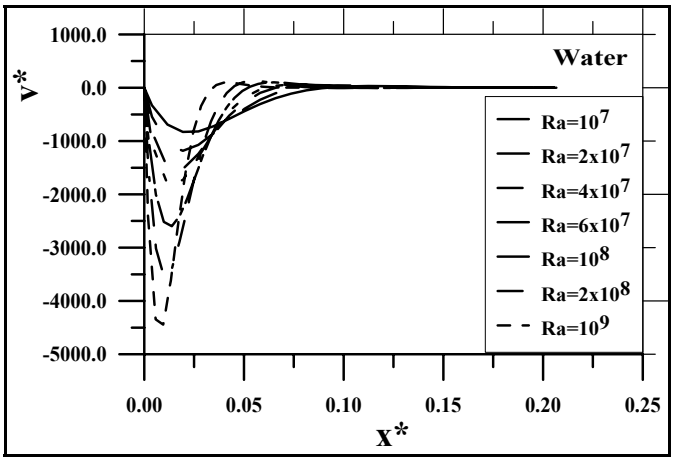

(b)

Figure 3: b)-Vertical Velocity distribution for high Rayleigh number regime.

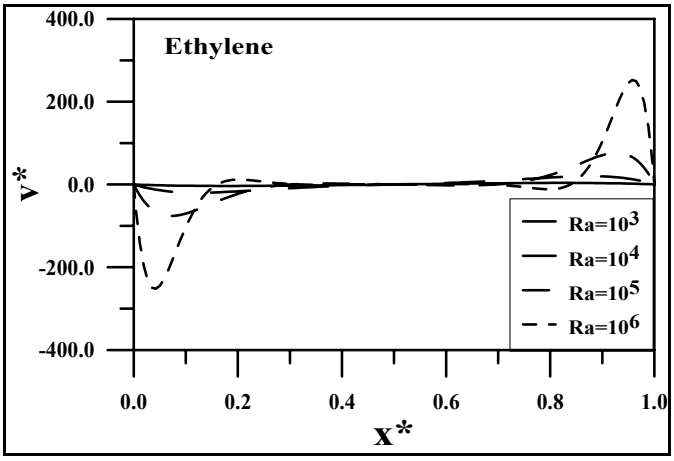

(a)

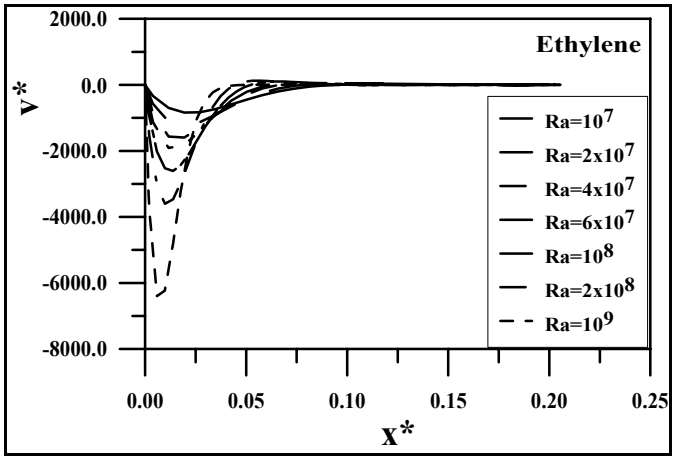

(b)

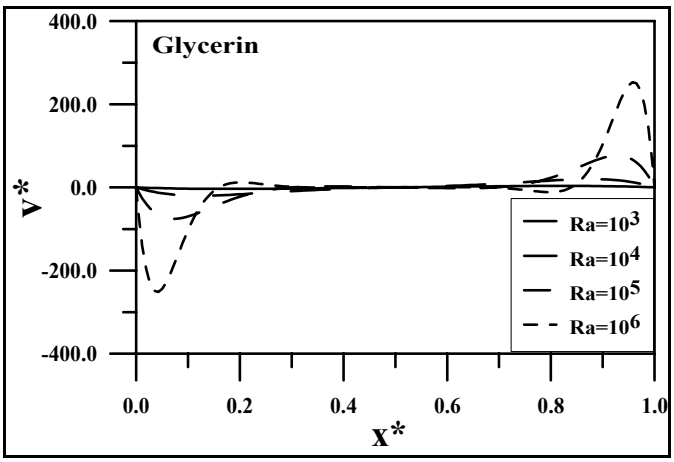

(a)

Figure 3: a)-Vertical Velocity distribution for low Rayleigh number regime.

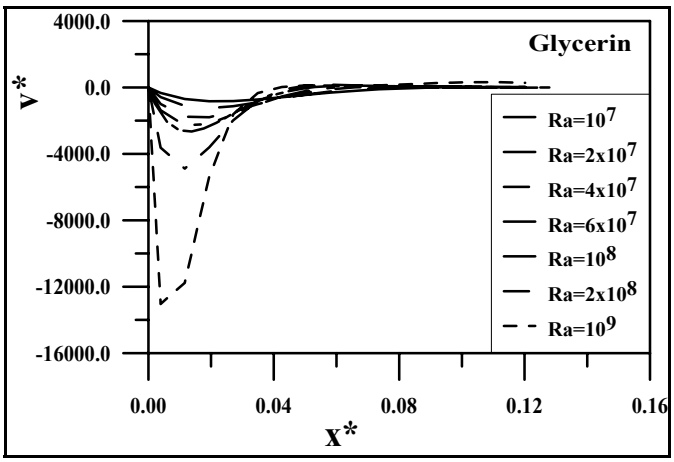

(b)

Figure 3: b)-Vertical Velocity distribution for high Rayleigh number regime.

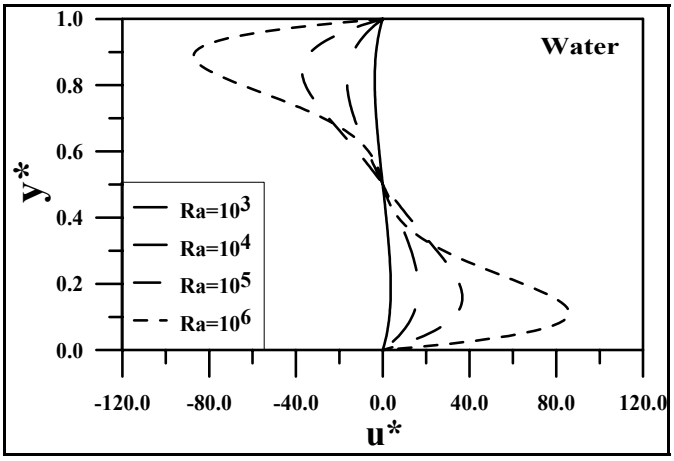

(a)

Figure4: a)-Sample horizontal Velocity Profile for Low Rayleigh number regimes.

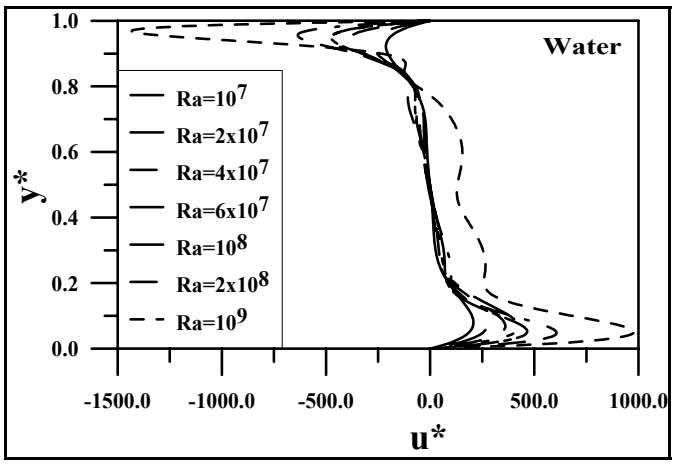

(b)

Figure 4: b)-Sample horizontal Velocity Profile for high Rayleigh number regimes.

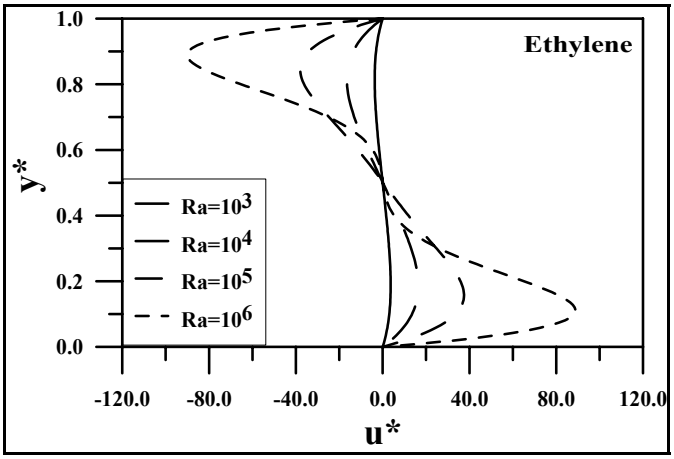

(a)

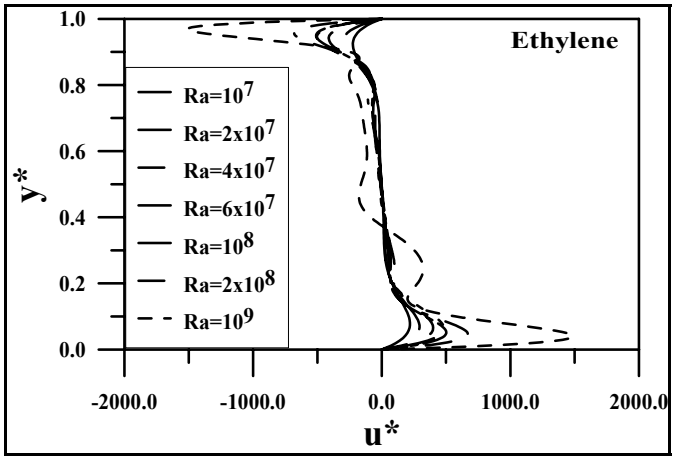

(b)

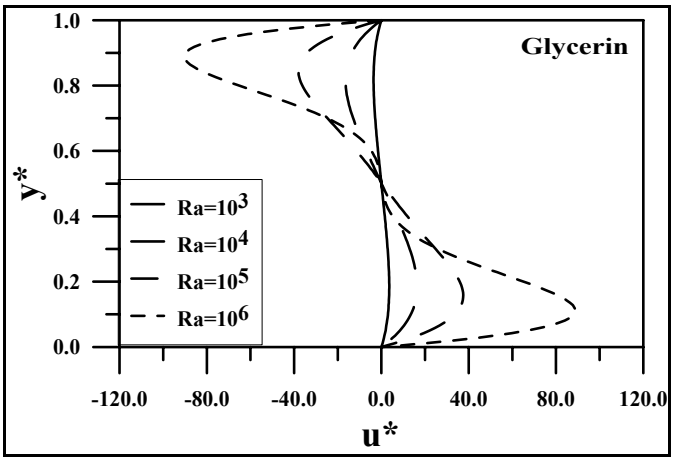

(a)

Figure 4: a)-Sample horizontal Velocity Profile for Low Rayleigh number regimes.

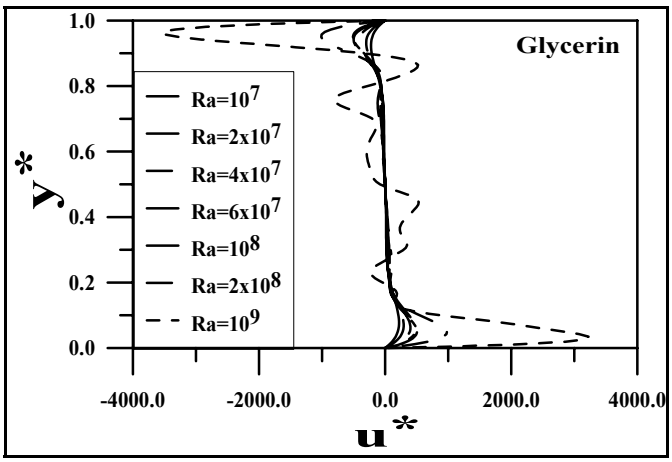

(b)

Figure 4: b)-Sample horizontal Velocity Profile for high Rayleigh number regimes.

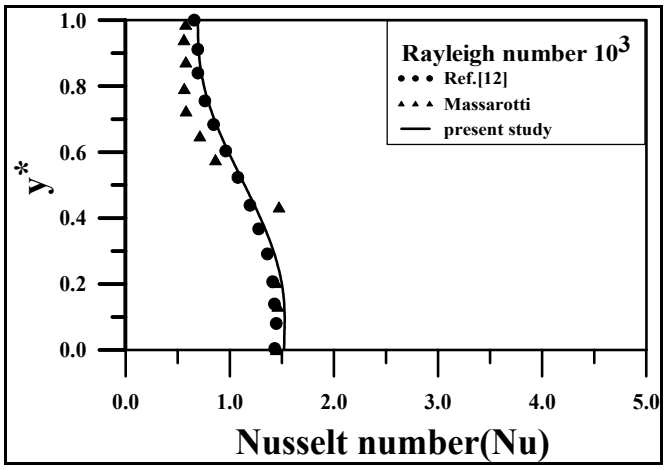

Figure 5: -Comparison of local Nusselt number of air along the Hot wall for $10^3 \leq Ra \leq 10^7$.

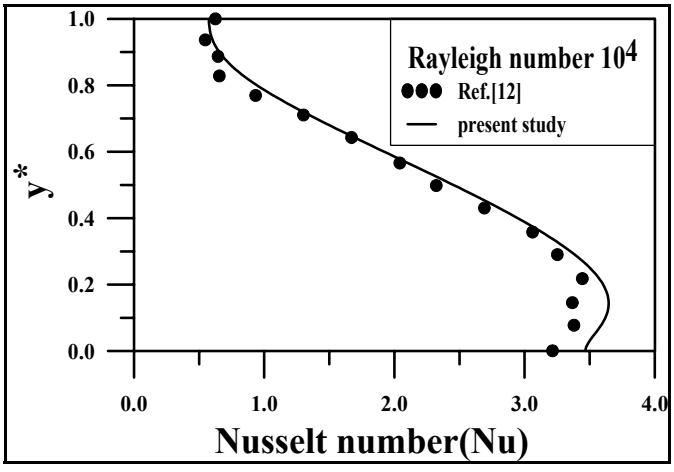

Figure 5: -Comparison of local Nusselt number of air along the Hot wall for $10^3 \leq Ra \leq 10^7$.

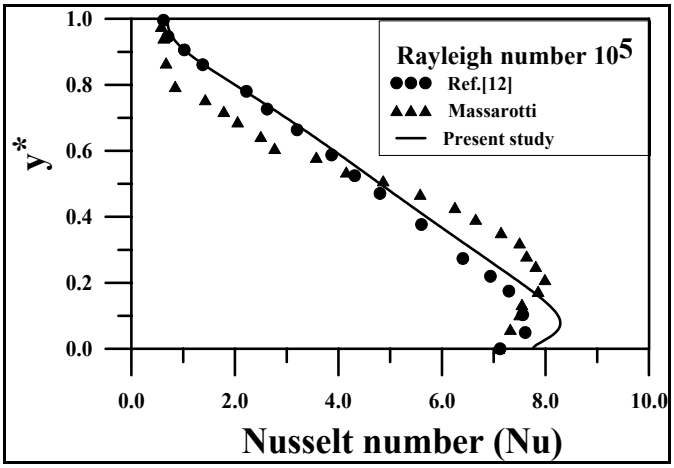

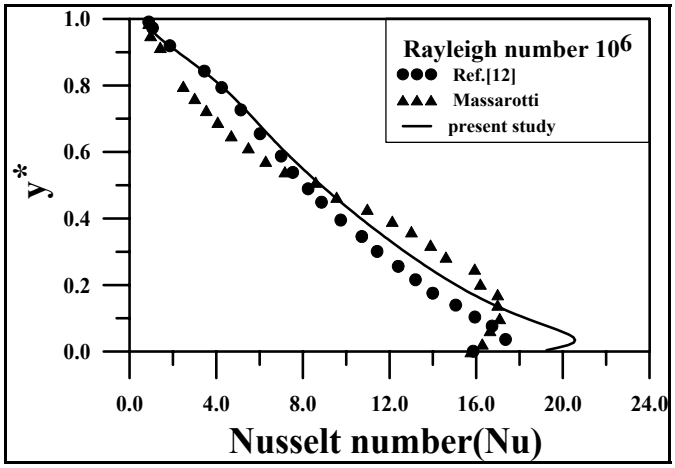

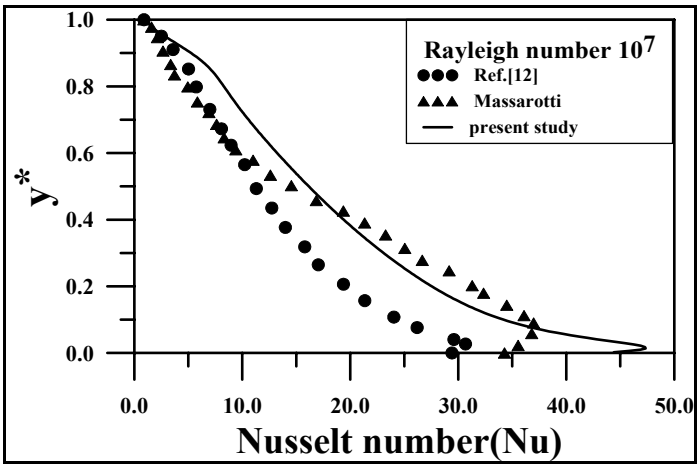

Figure 5: -Comparison of local Nusselt number of air Along the Hot wall for $10^3 \leq Ra \leq 10^7$.

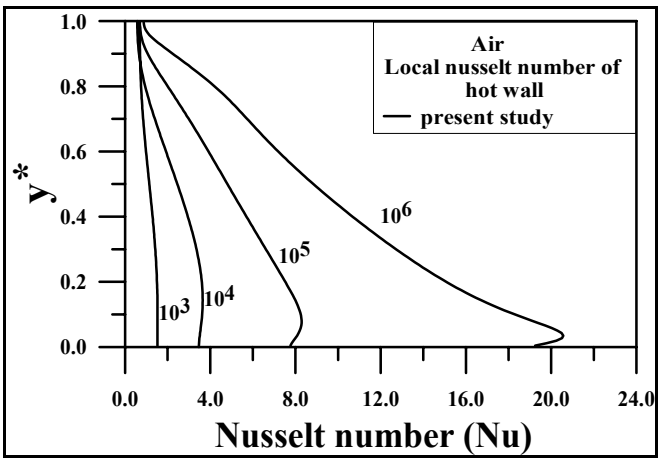

(a)

Figure 6: Local Nusselt number of air variation by FVM simulations: a) - hot wall, $10^3 \leq Ra \leq 10^6$

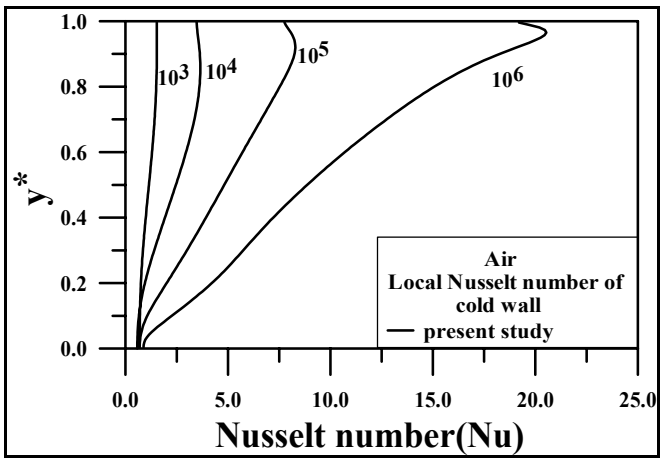

(b)

Figure 6: Local Nusselt number of air variation by FVM simulations: b) cold wall, $10^3 \leq Ra \leq 10^6$

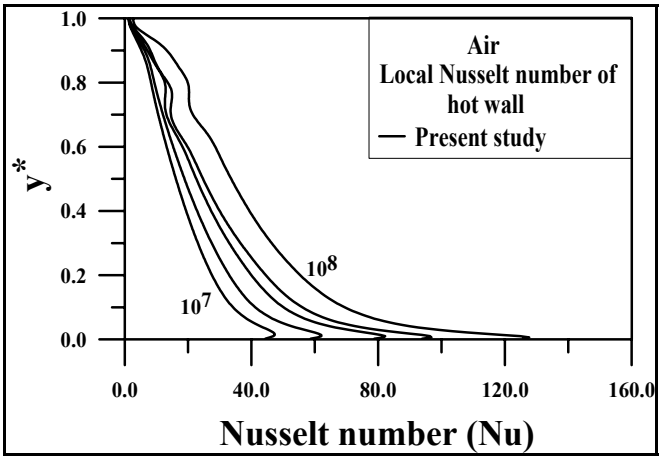

(a)

Figure 6: Local Nusselt number of air variation by FVM simulations: a)-hot wall, $10^7 \leq Ra \leq 10^8$.

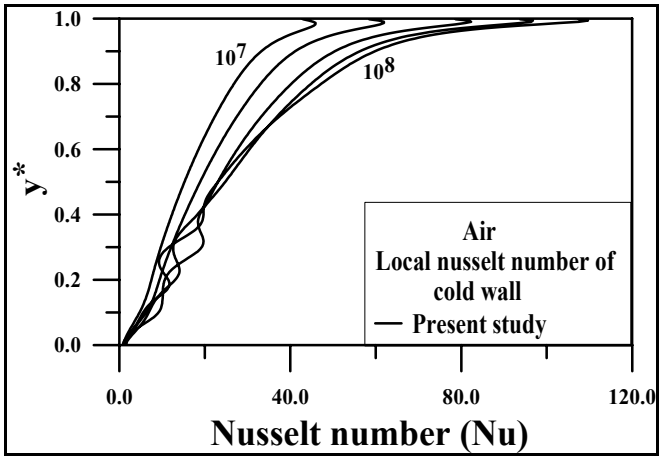

(b)

Figure 6: Local Nusselt number of air variation by FVM simulations: b) -cold wall, $10^7 \leq Ra \leq 10^8$.

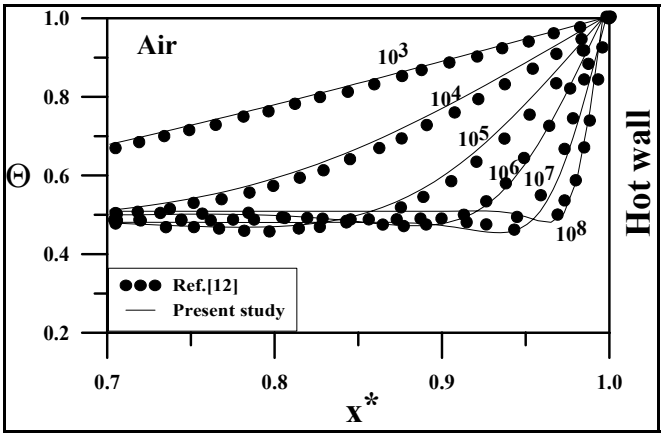

(a) Air

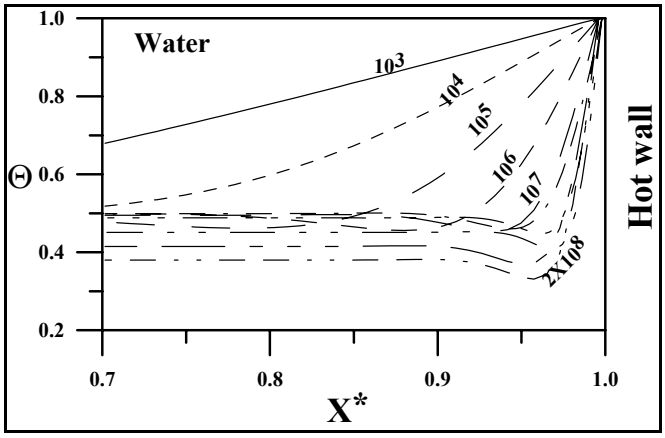

(b) Water

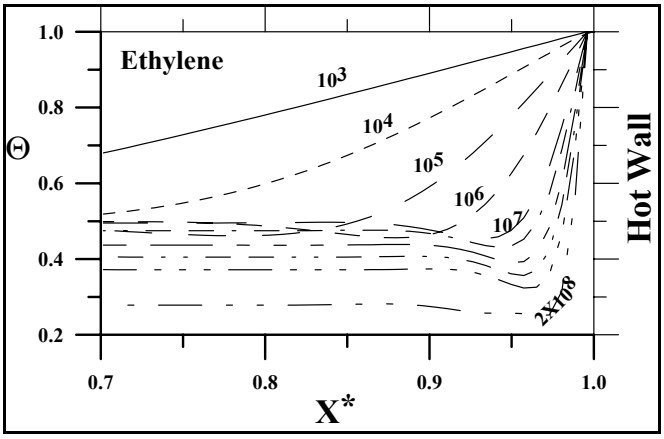

(c) Ethylene

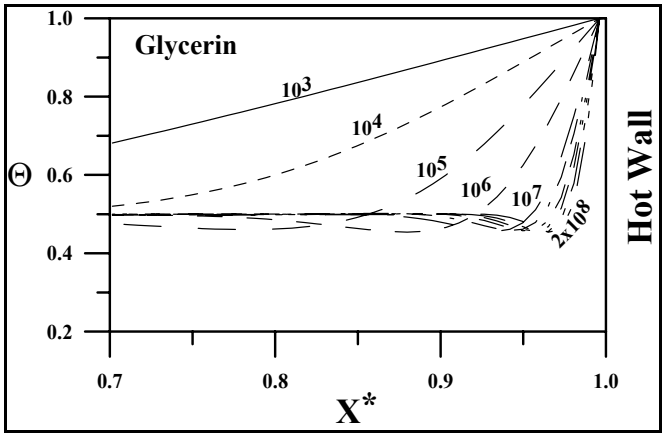

(d) Glycerin

Figure 7: Temperature distribution at the mid-height (y^*=0.5) near hot wall: a)-Air, b)-Water c)-Ethylene, d) Glycerin.